Cubic magnetic anisotropy in *B*20 magnets: Interplay of anisotropy and magnetic order in $Fe_{1-x}Co_xSi$

G. Gödecke [1,*] A. O. Leonov [2,3,†] J. Grefe [1] S. Süllow [1] and D. Menzel [1]

[1]*Institut für Physik der Kondensierten Materie, TU Braunschweig, D-38106 Braunschweig, Germany*

[2]*Department of Chemistry, Faculty of Science, Hiroshima University Kagamiyama, Higashi Hiroshima, Hiroshima 739-8526, Japan*

[3]*International Institute for Sustainability with Knotted Chiral Meta Matter (WPI-SKCM2), Hiroshima University, 1-3-1 Kagamiyama, Higashi-Hiroshima, Hiroshima 739-8526, Japan*

(Received 10 October 2025; revised 9 December 2025; accepted 27 February 2026; published 25 March 2026)

The metallic systems MnSi and $Fe_{1-x}Co_xSi$ are known to feature a generic magnetic phase diagram primarily determined by the isotropic exchange and Dzyaloshinskii-Moriya interactions. However, additional weaker anisotropies, lowest in the hierarchy of energy scales, play a crucial role: they determine the relative order of phases in the phase diagram and may even enable skyrmion stability far below the ordering temperature. Among cubic B20 helimagnets, the insulator Cu_2OSeO_3 is currently the only known example exhibiting a low-temperature, anisotropy-induced skyrmion pocket. In this manuscript, we present a systematic study of cubic magnetocrystalline anisotropy by means of angle-resolved SQUID magnetization measurements in MnSi and $Fe_{1-x}Co_xSi$ ($0.08 \leqslant x \leqslant 0.70$) single crystals and provide quantitative values of the anisotropy constants. For $Fe_{1-x}Co_xSi$, the cubic anisotropy is found to be strongly dependent on the Co concentration x. From a theoretical point of view, for low Co concentrations ($x \sim 0.10$), the anisotropy is expected to be sufficiently strong to stabilize a low-temperature skyrmion lattice. Therefore, $Fe_{1-x}Co_xSi$ may represent the first chiral metallic system to exhibit a low-temperature skyrmion phase controllably stabilized by cubic anisotropy for specific directions of the magnetic field.

DOI: 10.1103/h76w-8twm

I. INTRODUCTION

The *B*20 magnet MnSi has been established as a prototype chiral metal hosting a helimagnetic ground state and a rich magnetic phase diagram including the field-induced skyrmion lattice [1,2]. The principal interactions underlying the magnetic order in MnSi, i.e., a strong ferromagnetic exchange, intermediate antisymmetric exchanges, and weak cubic anisotropy, have been identified theoretically [3–5]. Extensive experiments aimed at these principal interactions have resulted in a well-established generic phase diagram [6–9]. MnSi undergoes a first-order phase transition into a helimagnetic ground state below $T_{HM} = 29.5$ K [10]. Applying an external field results in a transition from helical to conical ordering at the lower critical field H_{c1}. Further, above the higher critical field H_{c2}, the conical order completely field polarizes. Experiments show that for MnSi, the critical fields are only weakly dependent on the crystal orientation [3,8].

The isostructural doped semiconductor $Fe_{1-x}Co_xSi$ has also been subject to many studies regarding the same principal interactions for specific Co concentrations [11–16] and features the same generic phase diagram as MnSi [14–18]. However, in contrast to MnSi, the distinctive feature of the $Fe_{1-x}Co_xSi$ series is that key parameters such as ordering temperature, helical modulation length, spin-wave stiffness, Dzyaloshinskii-Moriya interaction strength, and cubic anisotropy can all be tuned systematically by varying the Co concentration, as demonstrated in a wide range of experiments [11,14,15,19–22]. This tunability over a wide Co concentration range makes the series $Fe_{1-x}Co_xSi$ an interesting platform for case studies, as opposed to MnSi influenced by external parameters such as pressure [23–26] or doped MnSi, where doping leads to the suppression of magnetic order already at low doping concentrations [19,20,27–32].

A schematic depiction of the phase diagram of $Fe_{1-x}Co_xSi$ as a function of the Co concentration x is shown in Fig. 1. For $x = 0.014$, the system undergoes a metal-to-insulator transition [22] from a correlated narrow-gap insulator featuring magnetic and conducting surface states [33,34] to bulk metallic behavior, closely followed by a nonmagnetic-to-magnetic phase transition at $x = 0.03$ [22]. Up to $x \sim 0.35$ the ordering temperature T_{HM} increases and exhibits a maximum at $T_{HM} \approx 53$ K. For high concentrations $x \sim 0.65$, a tendency to field polarize at very low fields has been reported [35], which is being attributed to vanishing asymmetric exchanges and finite cubic anisotropy. Above $x = 0.80$, long-range magnetic order vanishes.

Another key feature of MnSi and $Fe_{1-x}Co_xSi$ is the formation of a skyrmion lattice in a small region of the phase

*Contact author: g.goedecke@tu-braunschweig.de

†Contact author: leonov@hiroshima-u.ac.jp

Published by the American Physical Society under the terms of the Creative Commons Attribution 4.0 International license. Further distribution of this work must maintain attribution to the author(s) and the published article's title, journal citation, and DOI.

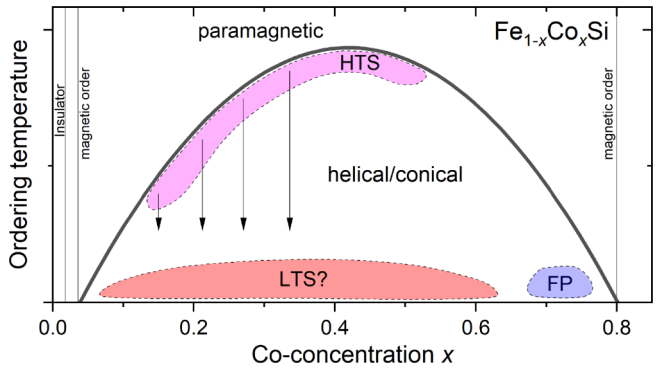


FIG. 1. Schematic depiction of the phase diagram of $Fe_{1-x}Co_xSi$ as function of the Co concentration x. At low Co concentrations, $Fe_{1-x}Co_xSi$ undergoes an insulator-to-metal transition, closely followed by a nonmagnetic-to-magnetic transition [22]. For Co concentrations up to $x = 0.50$, a high-temperature skyrmion phase (HTS) persists near T_{HM} [14–17] with a strong history dependence [17] as indicated by arrows. At high Co concentrations near $x \approx 0.65$ $Fe_{1-x}Co_xSi$ shows a tendency to show full field polarization (FP) [35]. From studies on Cu_2OSeO_3 [43,44], the question arises whether the tunable system $Fe_{1-x}Co_xSi$ also features a low-temperature skyrmion phase (LTS).

diagram near the ordering temperature [16,17], see Fig. 1. Though there have been efforts to characterize the cubic anisotropy and its influence on the formation of the skyrmion lattice in MnSi [36–38] and related compounds [39,40], there exists no systematic experimental study regarding the anisotropy in MnSi and $Fe_{1-x}Co_xSi$. This is mostly due to the fact that the anisotropy in MnSi and $Fe_{1-x}Co_xSi$ is weak and lowest in the energy hierarchy of the competing interactions, and has long been thought to only weakly orient the helix along the easy axes in zero field. Additionally, cubic anisotropy classically exhibits a strong temperature dependence such that the anisotropy vanishes much more rapidly than the ordered moment [41,42]. This makes it only more challenging to measure the anisotropy at temperatures in the vicinity of the fluctuation-induced skyrmion pocket in the phase diagram, which is referred to as the high-temperature skyrmion phase (HTS).

Recently, in the chiral insulating magnet Cu_2OSeO_3, a second skyrmion phase (LTS) has been identified at low temperatures far below the ordering temperature [43–46]. Cu_2OSeO_3 shares similar properties with MnSi and $Fe_{1-x}Co_xSi$, such as the lack of inversion symmetry and the resulting antisymmetric magnetic exchange interactions, leading to the same principal phase diagram: a helimagnetic ground state, transitions into a conical and field-polarized state at H_{c1} and H_{c2}, respectively, and a skyrmion phase near the ordering temperature [47,48]. However, in contrast to the fluctuation-induced high-temperature skyrmion phase, the low-temperature skyrmion phase is stabilized by cubic anisotropy and exhibits a pronounced directional dependence [43–46], pointing out a crucial role of anisotropy at low temperatures. This observation raises the question of whether such a secondary skyrmion phase may also exist in metallic MnSi and $Fe_{1-x}Co_xSi$, highlighting the need for a detailed understanding of cubic anisotropy in these systems. For a systematic investigation, the series $Fe_{1-x}Co_xSi$ provides a particular advantage, as parameters such as the cubic anisotropy can be tuned by varying the Co concentration. Further, a realization of an LTS phase in $Fe_{1-x}Co_xSi$ would open the door for numerous new experiments aimed at the transport properties of anisotropy-stabilized skyrmions.

In Ref. [44], the anisotropy of Cu_2OSeO_3 is estimated by magnetization measurements. It is shown that the anisotropy affects the noncollinear magnetic order with opposing signs under certain conical angles, i.e., the magnetization curves measured along the easy and hard axes exhibit a crossover [44]. This leads to a situation in which the anisotropy of Cu_2OSeO_3 is not easily measured by extracting the magnetization energy from zero magnetization to saturation. For MnSi, the magnetization curves feature no crossover, and for $Fe_{1-x}Co_xSi$, these effects play only a negligible role as can be seen by the angular dependence of the critical fields H_{c1} and H_{c2}, see below. Thus, for MnSi and $Fe_{1-x}Co_xSi$, the magnetic anisotropy may be determined by calculating the magnetization energy from angle-resolved magnetization measurements.

In this work, we not only aim at further narrowing down the field of uncharacterized magnetic interactions by measuring the cubic anisotropy of MnSi and $Fe_{1-x}Co_xSi$ but also identify promising Co concentrations that could host an LTS phase. We conduct angle-resolved magnetization measurements to obtain the magnetization energies and determine the anisotropy constants by fitting the data with a phenomenologically motivated function considering the overall cubic symmetry of the system. We then discuss the method of measuring magnetic anisotropy using magnetization measurements for the system $Fe_{1-x}Co_xSi$ by comparing the orientation dependence of the critical fields H_{c1} and H_{c2}. Determining the anisotropy constants leads to an extended phase diagram, which shows that magnetic order and cubic anisotropy in $Fe_{1-x}Co_xSi$ are not trivially connected. Putting anisotropy in the context of the critical field H_{c2} and the saturation magnetization M_s by calculating the unitless anisotropy constants, we show that relative anisotropy is strongest for Co concentrations where magnetic order emerges or vanishes, i.e., at the phase boundaries of the phase diagram. This method is complemented by the calculation of cubic anisotropy from theoretical simulations and values of H_{c2}. Comparison with a critical anisotropy threshold obtained from theoretical simulations leads to the identification of two promising Co concentrations by both aforementioned methods, likely to host a low-temperature skyrmion phase.

II. EXPERIMENTAL METHODS

For the experiments single crystals of MnSi and $Fe_{1-x}Co_xSi$ with Co concentrations $x = 0.08, 0.15, 0.20, 0.30, 0.50, 0.60, 0.65$, and 0.70 are grown by the tri-arc Czochralski method from a premelt of 99.99% Mn, 99.98% Fe, 99.95% Co, and Si ($\rho_n = 300$ Ωcm, $\rho_p = 3000$ Ωcm) in their respective stochiometric ratios. After growth, the crystals are Laue-oriented, and cube-shaped samples (~ 1 mm^3) are cut such that the cube edges align with the $\langle 100 \rangle$ cubic main axes of the crystal.

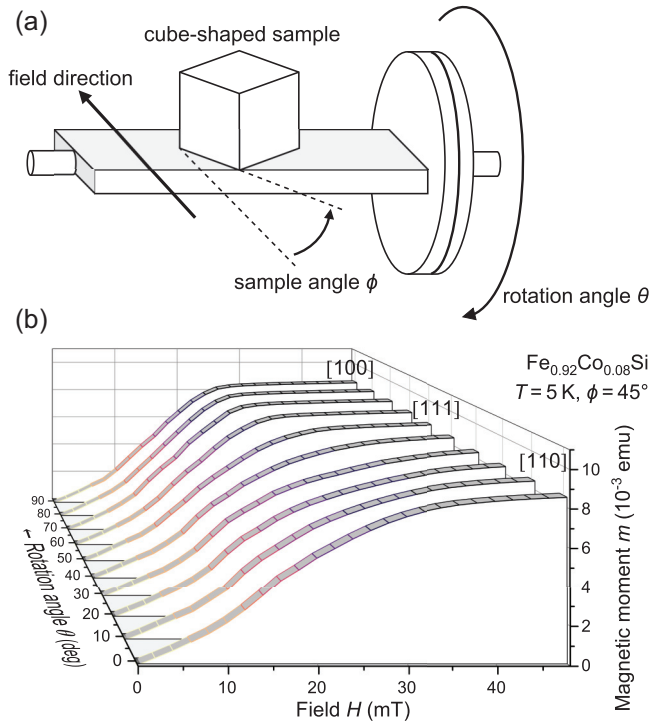


FIG. 2. (a) Rotatable sample holder used to conduct angle-resolved magnetization measurements and (b) exemplary measurements of the magnetic moment upon sample rotation for $Fe_{0.92}Co_{0.08}Si$ at $T = 5$ K. The magnetization direction relative to the crystal orientation is parametrized by the angles θ and ϕ.

The magnetic anisotropy is measured by means of angle-resolved magnetization measurements using a rotatable sample holder in a commercial SQUID magnetometer. The direction of the crystal lattice relative to the magnetic field is described by the sample angle ϕ and the rotation angle θ, see Fig. 2(a). The magnetization direction can be parametrized by a unit vector $\hat{\boldsymbol{m}} = \boldsymbol{M}/|\boldsymbol{M}| = (m_1, m_2, m_3) = (\sin\theta\cos\phi, \cos\theta, \sin\theta\sin\phi)$ in spherical coordinates where ϕ and θ are the azimuthal and the polar angle, respectively. The magnetization of all samples is measured up to saturation for multiple fixed sample angles and full rotations of the rotation angle in steps of 10°. Magnetization measurements are conducted for each rotation at $T = 5$ K and $T = 10$ K after heating beyond the respective ordering temperatures and cooling in zero-field to prevent history-dependent effects. Exemplary measurements for $Fe_{0.92}Co_{0.08}Si$ at $T = 5$ K for $\phi = 45°$ are shown in Fig. 2(b).

To distinguish between intrinsic and extrinsic contributions to the angular dependence of the magnetization, a geometric offset in the magnetization caused by the sample holder and the coil setup is taken into account. This offset exhibits a twofold symmetry which can be distinguished from cubic anisotropy by symmetry arguments and is typically of the order between $10^{-3}M_s$ and $10^{-4}M_s$. Additionally, the demagnetization tensors N of the different samples are calculated according to Ref. [49] from the sample dimensions. The internal magnetic field is then given by $\boldsymbol{H} = \boldsymbol{H}_{\text{ext}} - N \cdot \boldsymbol{M}$. The anisotropy can be characterized by calculating the magnetization energy E per unit volume

$$E(\hat{\boldsymbol{m}}) = \mu_0 \int_0^{M_s} \boldsymbol{H} \cdot \mathrm{d}\boldsymbol{M}, \tag{1}$$

as a function of the magnetization direction $\hat{\boldsymbol{m}}$ from the magnetization curve. As the $B20$ structure is cubic, the symmetry of the intrinsic magnetocrystalline anisotropy is also expected to be cubic. Here, we acknowledge that the local symmetry of the $B20$ unit cell is actually governed by tetrahedral symmetry; however, since the magnetization depends not strictly on a certain direction but rather on a respective directional axis, we consider overall cubic symmetry.

In a classical energy expansion for homogenously magnetized systems, cubic anisotropy is phenomenologically expressed in powers of direction components m_1, m_2, m_3 [50], such that the anisotropy energy can be described by

$$E_{\text{cub}}(\hat{\boldsymbol{m}}) = K_0 + K_1\left(m_1^2m_2^2 + m_2^2m_3^2 + m_1^2m_3^2\right) + \cdots. \tag{2}$$

As the cubic anisotropy of the B20 magnets is generally weak, the first nonvanishing term in the expansion is sufficient to describe the data, see below. Expansion terms of higher orders are neglected. The anisotropy is then solely characterized by the sign and magnitude of the fourth-order anisotropy constant K_1. The second-order anisotropy constant K_0, which is constant for cubic symmetry, includes all other isotropic contributions to the magnetization curve.

III. EXPERIMENTAL RESULTS

The magnetization energies E calculated from the magnetization curves according to Eq. (1) as a function of the crystal orientation for MnSi, $Fe_{0.92}Co_{0.08}Si$, $Fe_{0.50}Co_{0.50}Si$, and $Fe_{0.35}Co_{0.65}Si$ at selected sample angles are shown in Fig. 3. A general feature of all samples under investigation, except $Fe_{0.50}Co_{0.50}Si$, which will be discussed separately, is that all principal axes are energetically equivalent within the resolution of our experiment. This generally confirms cubic symmetry, i.e., the magnetization energies are the same for each ⟨100⟩ direction and further motivates the procedure of data fitting with Eq. (2) in cubic symmetry introduced in Sec. II.

Moreover, the evolution of the orientation-dependent magnetic behavior of MnSi and $Fe_{1-x}Co_xSi$ can be divided into four cases:

(i) For MnSi, the anisotropy constant K_1 is negative. The easy axes and, thus, minima in magnetization energy are along the ⟨111⟩ directions [Fig. 3(a)]. This is in agreement with literature as the easy axes have been inferred from neutron scattering data [6]. In zero field, the spin-helix vectors are aligned with the ⟨111⟩ directions.

(ii) For the low-doping regime in $Fe_{1-x}Co_xSi$ ($x \leqslant 0.30$) the anisotropy constant K_1 is positive. The easy axes are the ⟨100⟩ directions [Fig. 3(b)]. This is consistent with the helix vector in zero field aligned along the ⟨100⟩ directions as derived from neutron scattering experiments [14].

(iii) With increasing Co concentration, the anisotropy vanishes for $Fe_{0.50}Co_{0.50}Si$ within the experimental resolution. Figure 3(c) shows the magnetization energy upon rotating covering two ⟨100⟩ directions ([100] and [010]) and two ⟨110⟩ directions ([110] and $[\bar{1}10]$). For finite cubic anisotropy, each

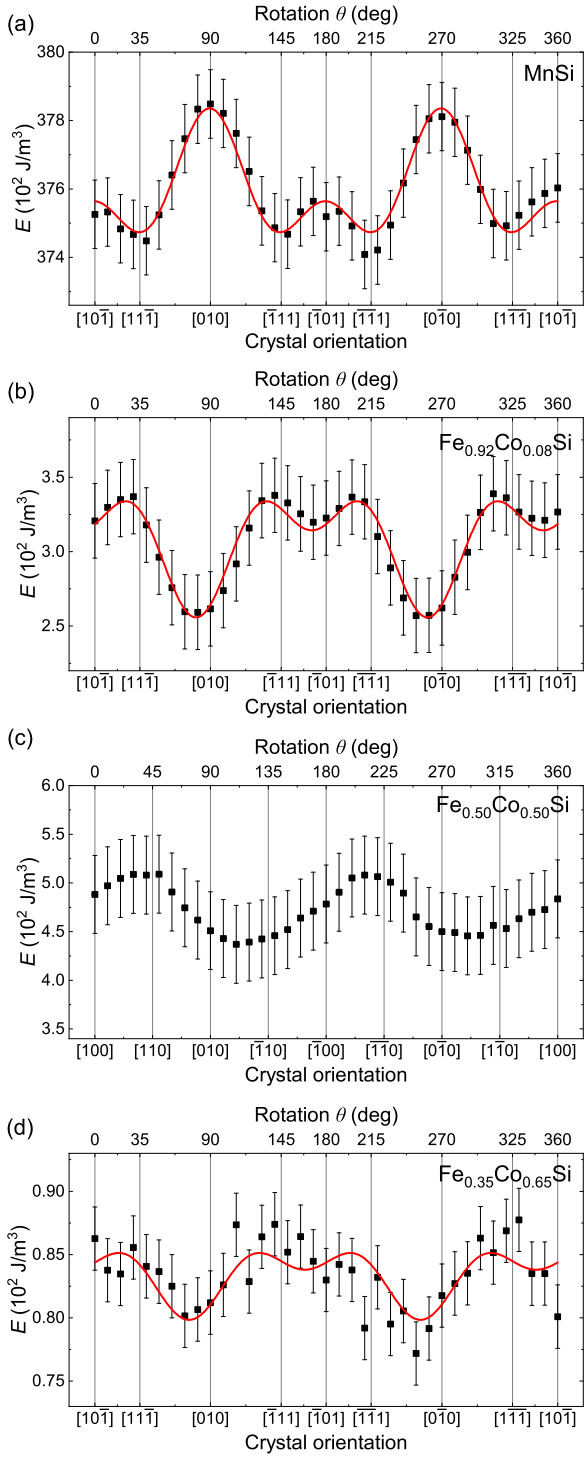


FIG. 3. Magnetization energies E as a function of the crystal orientation at $T = 5$ K for (a) MnSi with $\phi = 45°$, (b) $Fe_{0.92}Co_{0.08}Si$ with $\phi = 45°$, (c) $Fe_{0.50}Co_{0.50}Si$ with $\phi = 0°$, and (d) $Fe_{0.35}Co_{0.65}Si$ with $\phi = 45°$. Red lines represent the cubic anisotropy fit according to Eq. (2). (a) represents the case of $K_1 < 0$, (b) and (d) the case of $K_1 > 0$, and (c) $K_1 = 0$ within the resolution of our experiment.

⟨100⟩ direction and each ⟨110⟩ direction are expected to be energetically equivalent, exhibiting a fourfold symmetry. This is observed in our experiment for MnSi and other concentrations for $Fe_{1-x}Co_xSi$. In contrast, this is not the case for $Fe_{0.50}Co_{0.50}Si$, indicating vanishing cubic anisotropy, i.e., K_1 being zero. The residual orientation dependence is attributed to uncompensated demagnetization fields, which, however, can be distinguished from cubic anisotropy by the twofold symmetry.

(iv) In the high-doping regime for $Fe_{1-x}Co_xSi$ ($x \geqslant 0.60$), the cubic anisotropy recovers to finite values of K_1 [Fig. 3(d)]. However, the magnetization energies exhibit a far less pronounced orientation dependence than in the low-doping regime. The angular dependent magnetization energies are one order of magnitude weaker than for the low-doping regime. The data for all other Co concentrations with nonvanishing anisotropy is reminiscent of that of $Fe_{0.92}Co_{0.08}Si$, where only the magnitudes and, thus, the strength of the anisotropy, vary. In the high-doping regime, the energy scales of cubic anisotropy and demagnetization corrections become comparable, which leads to a reduced signal-to-noise ratio compared to the low-doping regime.

For a quantitative characterization of the magnetic anisotropy, the values of the anisotropy constants are determined by fitting the data according to Eq. (2) up to fourth order. To compensate for a slight misorientation of the rotation angle θ when initializing a measurement, the data is fitted considering a rotational offset θ_0 in the order of few degrees. The parameters K_0 and θ_0 are set as free fit parameters for each orientation ϕ. The parameter K_1 is a shared fit parameter across different orientations ϕ for each sample and temperature.

Conceptually, there is no reason for the anisotropy to be solely cubic and to be limited to only fourth order as used in Eq. (2). The energy expansion could feature terms of higher orders and include terms with a helix vector-orientation dependence. However, since all our measurements for different orientations at different temperatures show the equivalence of all ⟨111⟩, ⟨110⟩, and ⟨100⟩ directions, respectively, the inclusion of other expansion terms or fitting the data in sixth order is not motivated by our data. Additionally, fitting with more parameters only marginally improves the fit at the expense of an additional free parameter. Hence, we choose to neglect terms not included in Eq. (2).

Moreover, we emphasize that this approach does not resolve the individual contributions from spiral reorientation processes near H_{c1} and H_{c2}, possible skyrmion phases, or multidomain effects, all of which can influence the magnetization curves. Instead, the procedure effectively provides an average magnetic energy over these different spin configurations by using Eq. (2). Consequently, the extracted value of K_1 should be interpreted as a first-order estimate of the cubic anisotropy. A more accurate determination requires a comprehensive theoretical treatment that explicitly accounts for the actual spin textures, which will be discussed in subsequent analysis.

With the anisotropy constants K_1 derived at $T = 5$ K and $T = 10$ K for MnSi and $Fe_{1-x}Co_xSi$ a new phase diagram is obtained (Fig. 4). The total anisotropy is more pronounced for MnSi than for $Fe_{1-x}Co_xSi$ at $T = 5$ K and $T = 10$ K. For the system $Fe_{1-x}Co_xSi$, the general evolution shown in Fig. 3 is reflected in the anisotropy phase diagram, see Fig. 4. In the low-doping regime, the cubic anisotropy is finite with $K_1 > 0$. For $Fe_{0.50}Co_{0.50}Si$, however, the cubic anisotropy vanishes, while in the high doping regime, the cubic anisotropy is finite

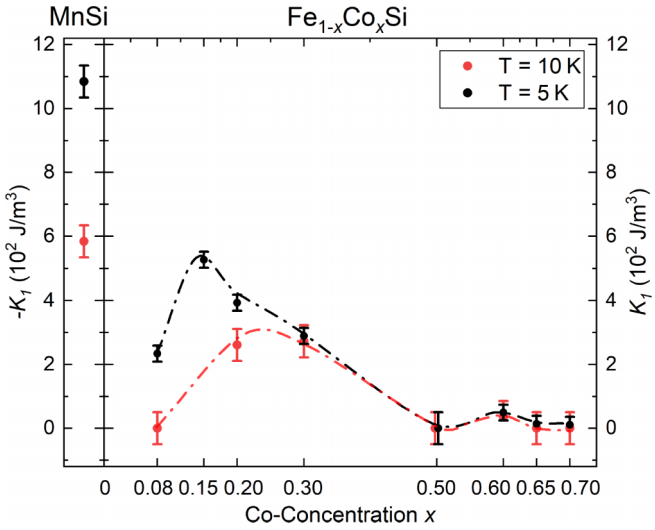


FIG. 4. Anisotropy constants $-K_1$ for MnSi and K_1 for $Fe_{1-x}Co_xSi$ ($0.08 \leqslant x \leqslant 0.70$) at $T = 5$ K and $T = 10$ K. Dashed lines are guides to the eye.

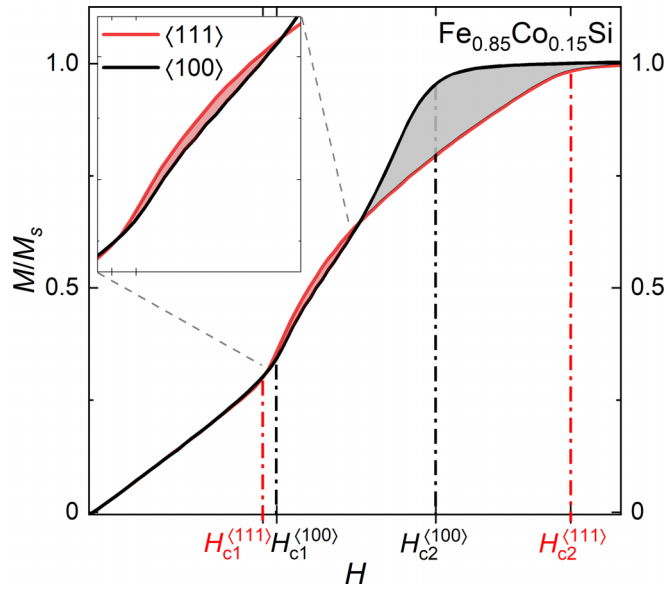


FIG. 5. Magnetization M for $Fe_{0.85}Co_{0.15}Si$ at $T = 5$ K along the ⟨100⟩ and ⟨111⟩ directions. The red-shaded region marks the area contributing with an opposite sign to the magnetic anisotropy (gray area). The critical fields are obtained from the first derivative and through linear interpolations near saturation.

with $K_1 > 0$ but about one order of magnitude weaker than for low doping. The highest total anisotropy at $T = 5$ K is observed for $Fe_{0.85}Co_{0.15}Si$.

The total values of the absolute anisotropy in MnSi and $Fe_{1-x}Co_xSi$ are more than one order of magnitude lower than in other skyrmionic compounds such as FeGe [51], Cu_2OSeO_3 [52], or $(Co_{0.5}Zn_{0.5})_{20-x}Mn_x$ [40]. The values of K_1 for MnSi are consistent with values reported in Ref. [53] when converting their results to our notation of Eq. (2) as $K_1 = -2K_1'$. Slight discrepancies are due to the use of a different experimental technique. In addition, data fitting with higher order expansion terms in Eq. (2) may lead to deviations as the expansion terms are nonorthogonal.

IV. DISCUSSION

A. Determination of cubic anisotropy from magnetization curves

Firstly, we want to discuss the validity of our method of determining the anisotropy constants from magnetization energies. Cubic anisotropies may be determined by a set of experiments, such as torque-magnetometry [51] or ferromagnetic resonance [40], all of which have some sort of drawback. However, magnetization measurements present the most readily available technique. But, as mentioned above, using Eq. (2) for an inhomogeneous magnet implies a form of averaging all spin structures, such as helicoids and skyrmions, from zero field up to saturation in a homogeneous approximation. This has the inherent flaw of not considering the formation of spin structures or reorientation processes, which also affect the magnetization curve. For example, as has been shown in Ref. [44], the critical fields in the system Cu_2OSeO_3 vary strongly with respect to the easy and hard axes. The magnetization along the easy and hard axes features a crossover between H_{c1} and H_{c2}, i.e., the magnetization is steeper for low fields along the hard axis, but the saturation occurs at lower fields along the easy axis. Thus, measuring the magnetization energy does not yield reliable values for the anisotropy constants in Cu_2OSeO_3. For $Fe_{1-x}Co_xSi$, however, these effects are less pronounced. As shown in Fig. 5, the magnetization of $Fe_{0.85}Co_{0.15}Si$ does show a crossover between H_{c1} and H_{c2} for the easy and hard axes but the crossover region (red shaded area) is much smaller than the difference induced by the cubic anisotropy (gray shaded area). The crossing region contributes with an opposing sign to the net measured anisotropy. By calculating the ratio of the contributing red and gray areas in the magnetization curve, the error can be estimated to be around 1%–2%.

This crossover can be visualized by the directional dependence of the critical fields for $Fe_{0.85}Co_{0.15}Si$, shown in Fig. 6(a). The critical field H_{c1} is determined as the first maximum of the magnetization curve derivative dM/dH. The values of the critical field H_{c2} are obtained by determining the intersection of the linear extrapolation of the magnetization curve between H_{c1} and saturation and beyond saturation. For $Fe_{1-x}Co_xSi$ at low Co concentrations ($x \leqslant 0.20$), the critical field H_{c1} is maximal along the easy axes and shows a minimum along the hard axes. The critical field H_{c2} shows the exact opposite behavior, which leads to a crossover in magnetization shown in Fig. 5. For higher concentrations $x \geqslant 0.30$, this crossover in magnetization is not observable in our measurements as the critical field H_{c1} becomes essentially isotropic. For MnSi, however, there does not exist a crossover in the magnetization, and the critical fields show the same angular dependence as shown in Fig. 6(b). From these findings, it can be assumed that at least for $Fe_{1-x}Co_xSi$ ($x \leqslant 0.20$), our values for K_1 are slightly underestimated, but the measurements for higher concentrations and MnSi are essentially unaffected by these effects. Thus, although being approximate, this approach yields a first-order estimate of the

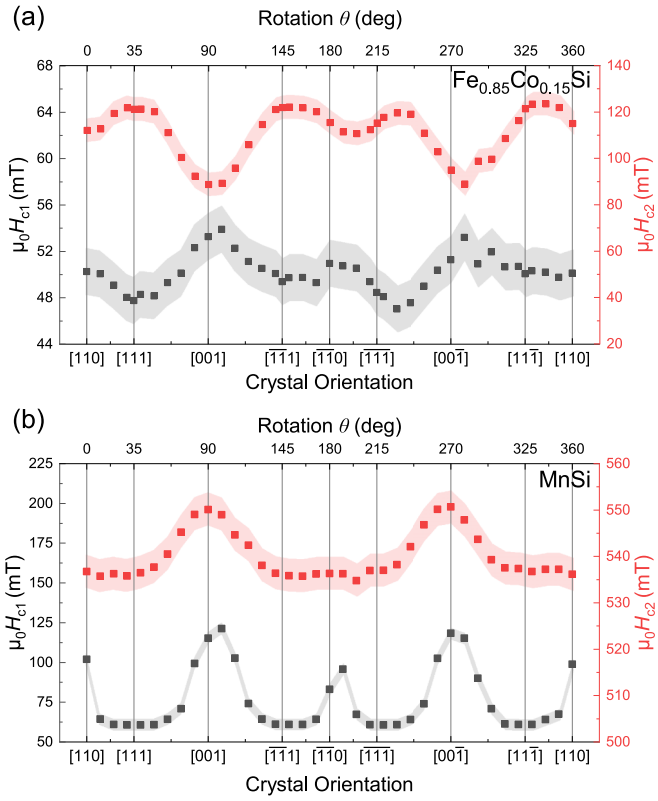


FIG. 6. Critical fields H_{c1} and H_{c2} as a function of the crystal orientation at $T = 5$ K for (a) $Fe_{0.85}Co_{0.15}Si$ and (b) MnSi. Values for H_{c1} and H_{c2} have been corrected by subtracting the projected demagnetization field. Shaded regions are errors governed by finite field increments during the measurements.

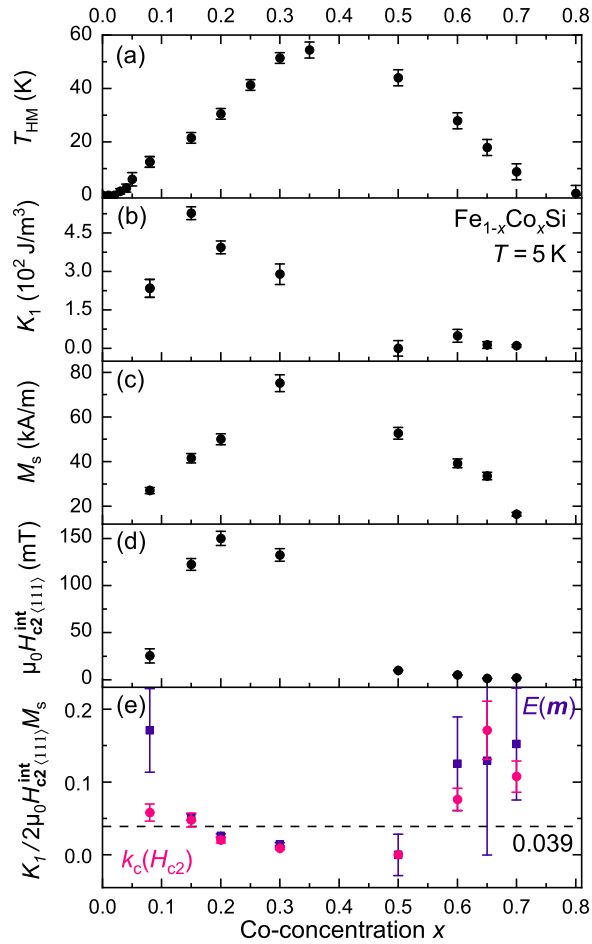


FIG. 7. (a) Magnetic ordering temperatures T_{HM}, (b) anisotropy constant K_1, (c) saturation magnetization M_s, (d) internal critical field $H^{int}_{c2\langle 111\rangle}$, and (e) unitless anisotropy k_c from magnetization energies (purple symbols) and H_{c2} (pink symbols) at $T = 5$ K for $Fe_{1-x}Co_xSi$ as a function of the Co concentration x. The threshold for LTS stabilization at $k_c = 0.039$ according to Fig. 8(a) is highlighted.

cubic anisotropy. The validity of the method is again reflected by our values of the anisotropy constants for MnSi being close to values reported in Ref. [53] using a different experimental technique that is unaffected by these features in the magnetization.

B. Co concentration dependence and low-temperature skyrmions in $Fe_{1-x}Co_xSi$

To put our findings into the context of magnetic order in the system $Fe_{1-x}Co_xSi$, the ordering temperatures and anisotropy constants at $T = 5$ K across the whole magnetic doping range are summarized in Figs. 7(a) and 7(b). The ordering temperature and anisotropy constant both feature maxima that do not coincide, and the evolution of the anisotropy as a function of the concentration does not resemble the trend of the ordering temperatures. We conclude that magnetic order and cubic anisotropy are not trivially dependent on each other. This can be easily understood when considering the respective energy scales. The values of the ordering temperatures are of the order of tens of Kelvin, resulting in an order of a few meV of magnetic exchange energies. Compared to that, if we consider the total cubic anisotropy per metal atom, we obtain an approximate energy of the order 10^{-4} meV, again emphasizing the stark difference in energy scales. Further, for $Fe_{1-x}Co_xSi$, the nonmonotonic evolution of the anisotropy as a function of x is best explained by the itinerancy of the metallic system. In itinerant magnets, anisotropy is strongly dependent on band-filling and, thus, doping [54].

Although anisotropy and magnetic order appear to be largely decoupled, it is nevertheless useful to characterize the strength of the cubic anisotropy relative to the physical quantities defining the magnetic order. For this purpose, we introduce the dimensionless anisotropy constant k_c, defined in terms of the exchange stiffness A and the Dzyaloshinskii-Moriya interaction coefficient D, or equivalently through the critical field and saturation magnetization,

$$k_c = K_1 \frac{A}{D^2} = \frac{K_1}{2\mu_0 H_{c2} M_s}. \tag{3}$$

The advantages of introducing this dimensionless parameter can be summarized as follows.

First, the anisotropy parameter k_c emerges naturally within the phenomenological Dzyaloshinskii theory written in nondimensional units

$$w = WA/D^2 = (\nabla \mathbf{m})^2 + \mathbf{m} \cdot (\nabla \times \mathbf{m}) - \mathbf{m} \cdot \mathbf{h} + k_c\left(m_1^2 m_2^2 + m_1^2 m_3^2 + m_2^2 m_3^2\right). \tag{4}$$

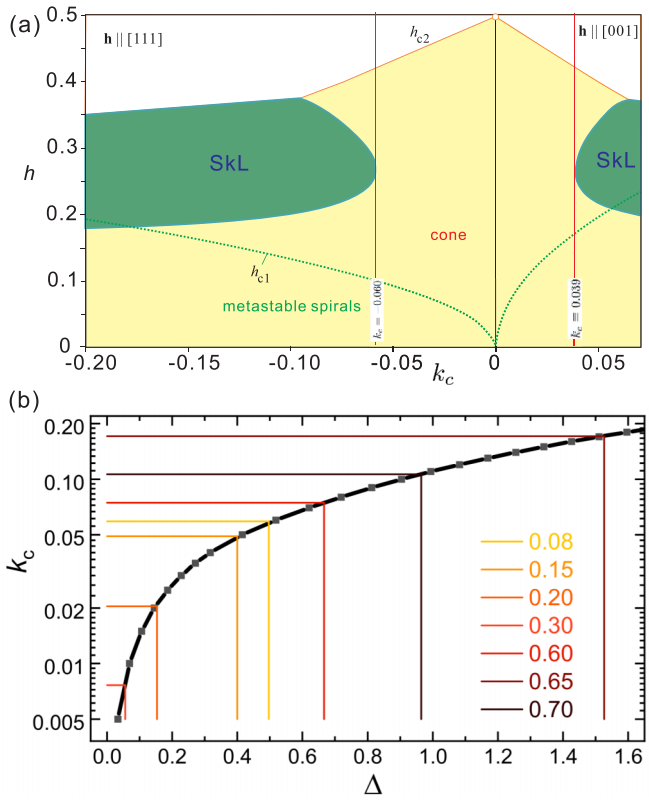


FIG. 8. (a) Phase diagram obtained from numerical simulations in the Dzyaloshinskii framework, see [55] for details, showing region of LTS stabilization as a function of the unitless anisotropy constant k_c. (b) Dimensionless anisotropy k_c for $Fe_{1-x}Co_xSi$ as a function of the parameter Δ inferred from numerical simulations in the Dzyaloshinskii framework, see [55]. Values for Δ and k_c for the different Co concentrations are marked by solid lines. The sample with $x = 0.50$ is not shown, as the critical field H_{c2} is isotropic in the resolution of our experiments.

Here, the nondimensional energy density w is expressed as the sum of the exchange, DMI, Zeeman, and anisotropy contributions. Together with the dimensionless magnetic field $h = HAM_s/D^2$, the parameter k_c acts as a fundamental control parameter of the model.

Second, by casting the theory in nondimensional form, we significantly reduce the number of independent parameters. In contrast, the dimensional energy density W contains several material-specific quantities that are often not known with sufficient accuracy. Thus, the use of nondimensional parameters renders the results more general and allows a unified description of many physical systems within the same phenomenological framework. The reduced parameter set facilitates a more transparent analysis of how solutions depend on key dimensionless ratios, without the need to vary each physical constant individually.

The resulting phase diagrams—plotted in the (k_c, h) plane—map out the regions of oblique spirals, the conical state, and skyrmion phases, and determine the corresponding critical fields h_{c1} and h_{c2} for an arbitrary direction of the applied magnetic field. Figure 8(a) shows the phase diagrams for both signs of k_c and for two representative field directions chosen to maximize the stability range of the skyrmion phase. Notably, the threshold values $k_c = 0.039$ for easy $\langle 001 \rangle$ axes and $k_c = -0.060$ for easy $\langle 111 \rangle$ axes mark the emergence of the skyrmion lattice in the respective anisotropy regimes (see Ref. [55] for details).

If one wishes to apply the simulation results to a specific compound, the corresponding nondimensional units can be readily computed, enabling the identification of the appropriate parameter point on the theoretical phase diagram.

In Fig. 7(e) (purple symbols), we plot the ratio (3) $K_1/2\mu_0 H^{\rm int}_{c2\langle 111\rangle} M_s$ obtained from our experiments. For the critical field, we again use the internal magnetic field in which the appropriate projected demagnetization field has been subtracted. The corresponding saturation magnetization and critical fields are shown in Figs. 7(c) and 7(d). The threshold value $k_c = 0.039$ is indicated by the dashed line in Fig. 7(e).

It is evident that in the low-doping regime the samples with $x = 0.08$ and 0.15 exhibit a sizable dimensionless anisotropy, sufficient to stabilize skyrmions at low temperatures. Taking into account the experimental requirements regarding achievable temperatures and field stability-namely, maximizing H_{c2} and $T_{\rm HM}$-the compound $Fe_{0.85}Co_{0.15}Si$ emerges as the most promising platform for searching for the LTS phase at low temperatures.

We also note that the values of H_{c2} and M_s extracted from our measurements are in good agreement with the literature [14,15,17,19–21]. When considering the unitless anisotropy as a function of Co concentration, it becomes apparent that well within the phase boundaries of magnetic order the magnetic anisotropy remains very weak compared to the other magnetic interactions, as reflected by the dimensionless anisotropy remaining close to zero. Interestingly, however, near the phase boundaries where magnetic order either emerges or disappears, the anisotropy increases significantly relative to H_{c2} and M_s. At these boundaries—i.e., for very low or very high doping—the magnetic anisotropy at low temperatures becomes comparable to the other magnetic exchange interactions.

Regarding the high-doping regime, it should be noted that the errors at high concentrations are governed by the aforementioned worsened signal-to-noise ratio in magnetization energies leading to errors in values of K_1, and because of the low values of H_{c2} along the hard axes, demagnetization corrections are comparable to the values of H_{c2}. Because of the very low H_{c2} fields there exist similarities to the situation reported for the related compound $Fe_{1-x}Co_xGe$ [56], where, at a certain critical concentration, the Dzyaloshinskii-Moriya interaction vanishes and the combination of ferromagnetic exchange with cubic anisotropy results in full field polarization. Compared to literature, the gain in relative anisotropy at high Co concentrations for $Fe_{1-x}Co_xSi$ may be the cause of the tendency to field-polarize at very low fields, as inferred from neutron scattering data [35], indicating a vanishing antisymmetric contribution and the interplay of ferromagnetic exchange and strong cubic anisotropy. From the experimental point of view, finding low-temperature skyrmions in a field range comparable to the internal H_{c2} of a few mT seems unlikely in comparison to the low Co concentrations.

C. Anisotropy determined from numerical simulations and H_{c2}

As has been mentioned above, the method of extracting quantitative values of the anisotropy by magnetization energies does not fully take contributions to the magnetization curve from the different nonhomogeneous spin states into account. Especially when trying to predict low-temperature skyrmion stability in a narrow parameter range, these deviations might play a role such that the magnetization energy approach should not be the sole method for determining anisotropies. This motivates a more thorough approach from the theoretical side, where domain effects and reorientation processes can be considered. For that, again, the phenomenological Dzyaloshinskii model, see Eq. (4), can be deployed to numerically simulate the critical fields h_{c1} and h_{c2} depending on the unitless anisotropy constant k_c.

For the subsequent analysis of experimental magnetization curves, we introduce a parameter Δ that quantifies the difference between the maximal dimensionless critical field h_{c2} along the hard axis and the minimal dimensionless critical field along the easy axis, normalized by the lowest critical field [55]. For $k_c > 0$, the theoretical parameter Δ takes the form

$$\Delta = \frac{h_{c2[111]} - h_{c2[100]}}{h_{c2[100]}}. \tag{5}$$

The same quantity Δ can be directly obtained from experimental values of the critical fields

$$\Delta = \frac{H_{c2[111]} - H_{c2[100]}}{H_{c2[100]}}. \tag{6}$$

Although the latter formula uses the dimensional values of the fields, the parameter Δ is itself nondimensional and provides a convenient quantitative measure of the effectiveness of the cubic anisotropy.

Thus, once Δ is determined experimentally, one can immediately infer the corresponding value of k_c used in the Dzyaloshinskii model (4), without requiring explicit knowledge of the full set of material parameters for the sample.

Figure 8(b) establishes the correspondence between the experimentally accessible parameter Δ and the nondimensional cubic anisotropy constant k_c. The resulting values of k_c obtained through this mapping are shown as pink symbols in Fig. 7(e), in contrast to the purple points extracted directly from the magnetic energy analysis presented in the previous sections.

Strikingly, the nondimensional anisotropy parameters k_c inferred from different approaches coincide for most samples in our study. This highlights the applicability of both methods as they seem to yield similar results from two very different starting points, one being theoretical and the other experimental. Additionally, regarding the threshold of $k_c = 0.039$, both methods indicate the potential stability of low-temperature skyrmion phases for $Fe_{1-x}Co_xSi$ at very low and very high Co concentrations. However, as discussed above, the findings for the high-doping regime are best interpreted as in Ref. [35] and the experimental realisation of an LTS phase at such low critical fields seems unlikely.

However, there exist discrepancies for the $x = 0.08$ sample in Fig. 7(e) for both methods, where the value determined by $E(\hat{\boldsymbol{m}})$ exceeds the one based on H_{c2}. This most likely has two main contributions: for one, the values of H_{c2} are small and only determined with some margin of error as demagnetization corrections become comparable. On the other hand, the saturation magnetization for $Fe_{1-x}Co_xSi$ is not always easily measured. For all samples, the magnetic moment does not fully saturate, even at moderately high fields [22,57]. However, for most samples, the magnetization flattens considerably above H_{c2}, which can be used as a value for the saturation magnetization. But this does not hold in the vicinity of the quantum critical point $x \approx 0.03$ [22], as is the case for the $x = 0.08$ sample, where the magnetization curve does not fully flatten, leading to an underestimation of the saturation magnetization and thus an overestimation of k_c calculated from Eq. (3).

D. Possibility of low-temperature skyrmions in MnSi

Though the role of MnSi in this manuscript is to demonstrate the case of a negative cubic anisotropy constant, we lastly want to shortly discuss the feasibility of an LTS phase in MnSi. The absolute value of the cubic anisotropy constant in MnSi is bigger than in $Fe_{1-x}Co_xSi$, however, calculating k_c from $E(\hat{\boldsymbol{m}})$ and H_{c2} yields $k_c = -0.0075$ and $k_c = -0.0044$, respectively. As can be seen from Fig. 8(a), a threshold of $k_c = -0.060$ would need to be fulfilled for negative values of k_c. The absolute value of the unitless anisotropy obtained from both methods is about one order of magnitude smaller, rendering a low-temperature skyrmion phase in MnSi unlikely.

V. CONCLUSIONS

Summarizing our findings, we have shown that angle-resolved magnetization measurements present a viable technique to quantitatively measure total cubic anisotropies in itinerant systems such as MnSi and $Fe_{1-x}Co_xSi$. Further, with the use of this technique, we have established an anisotropy phase diagram for $Fe_{1-x}Co_xSi$ across the whole magnetic doping range, having identified characteristic doping regimes. Putting the anisotropy in the context of magnetic order, cubic anisotropy seems to be decoupled from the ordered moment due to the steep energy hierarchy. When considering a unitless anisotropy relative to the exchange energies represented by H_{c2} and the ordered moment M_s, we have identified regions with strong relative anisotropy at the phase diagram boundaries where magnetic order emerges/vanishes. This is in overall good agreement with dimensionless anisotropies calculated from values of H_{c2} and numerical simulations. Compared to theory, the relative anisotropy constants determined from magnetization curves and H_{c2} for $x = 0.08$ and 0.15 exceed a theoretically needed threshold. This suggests that a secondary skyrmion phase at low temperatures may in principle be possible for low Co concentrations in $Fe_{1-x}Co_xSi$.

ACKNOWLEDGMENT

We acknowledge fruitful discussions with U. K. Rößler and comments from A. Rosch.

DATA AVAILABILITY

The data that support the findings of this article are not publicly available upon publication because it is not technically feasible and/or the cost of preparing, depositing, and hosting the data would be prohibitive within the terms of this research project. The data are available from the authors upon reasonable request.

[1] S. Mühlbauer, B. Binz, F. Jonietz, C. Pfleiderer, A. Rosch, A. Neubauer, R. Georgii, and P. Böni, Skyrmion lattice in a chiral magnet, Science **323**, 915 (2009).

[2] A. Neubauer, C. Pfleiderer, B. Binz, A. Rosch, R. Ritz, P. G. Niklowitz, and P. Böni, Topological Hall effect in the *A* phase of MnSi, Phys. Rev. Lett. **102**, 186602 (2009).

[3] Y. Ishikawa, K. Tajima, D. Bloch, and M. Roth, Helical spin structure in manganese silicide MnSi, Solid State Commun. **19**, 525 (1976).

[4] P. Bak and M. H. Jensen, Theory of helical magnetic structures and phase transitions in MnSi and FeGe, J. Phys. C **13**, L881 (1980).

[5] O. Nakanishi, A. Yanase, A. Hasegawa, and M. Kataoka, The origin of the helical spin density wave in MnSi, Solid State Commun. **35**, 995 (1980).

[6] S. V. Grigoriev, S. V. Maleyev, A. I. Okorokov, Y. O. Chetverikov, P. Böni, R. Georgii, D. Lamago, H. Eckerlebe, and K. Pranzas, Magnetic structure of MnSi under an applied field probed by polarized small-angle neutron scattering, Phys. Rev. B **74**, 214414 (2006).

[7] S. V. Grigoriev, S. V. Maleyev, A. I. Okorokov, Y. O. Chetverikov, and H. Eckerlebe, Field-induced reorientation of the spin helix in MnSi near T_c, Phys. Rev. B **73**, 224440 (2006).

[8] A. Bauer and C. Pfleiderer, Magnetic phase diagram of MnSi inferred from magnetization and ac susceptibility, Phys. Rev. B **85**, 214418 (2012).

[9] A. Bauer, M. Garst, and C. Pfleiderer, Specific heat of the skyrmion lattice phase and field-induced tricritical point in MnSi, Phys. Rev. Lett. **110**, 177207 (2013).

[10] M. Janoschek, M. Garst, A. Bauer, P. Krautscheid, R. Georgii, P. Böni, and C. Pfleiderer, Fluctuation-induced first-order phase transition in Dzyaloshinskii-Moriya helimagnets, Phys. Rev. B **87**, 134407 (2013).

[11] J. Beille, J. Voiron, F. Towfiq, M. Roth, and Z. Y. Zhang, Helimagnetic structure of the $Fe_xCo_{1-x}Si$ alloys, J. Phys. F: Met. Phys. **11**, 2153 (1981).

[12] J. Beille, J. Voiron, and M. Roth, Long period helimagnetism in the cubic B20 $Fe_xCo_{1-x}Si$ and $Co_xMn_{1-x}Si$ alloys, Solid State Commun. **47**, 399 (1983).

[13] M. Motokawa, S. Kawarazaki, H. Nojiri, and T. Inoue, Magnetization measurements of $Fe_{1-x}Co_xSi$, J. Magn. Magn. Mater. **70**, 245 (1987).

[14] S. V. Grigoriev, V. A. Dyadkin, D. Menzel, J. Schoenes, Y. O. Chetverikov, A. I. Okorokov, H. Eckerlebe, and S. V. Maleyev, Magnetic structure of $Fe_{1-x}Co_xSi$ in a magnetic field studied via small-angle polarized neutron diffraction, Phys. Rev. B **76**, 224424 (2007).

[15] S. V. Grigoriev, S. V. Maleyev, V. A. Dyadkin, D. Menzel, J. Schoenes, and H. Eckerlebe, Principal interactions in the magnetic system $Fe_{1-x}Co_xSi$: Magnetic structure and critical temperature by neutron diffraction and SQUID measurements, Phys. Rev. B **76**, 092407 (2007).

[16] W. Münzer, A. Neubauer, T. Adams, S. Mühlbauer, C. Franz, F. Jonietz, R. Georgii, P. Böni, B. Pedersen, M. Schmidt, A. Rosch, and C. Pfleiderer, Skyrmion lattice in the doped semiconductor $Fe_{1-x}Co_xSi$, Phys. Rev. B **81**, 041203 (2010).

[17] A. Bauer, M. Garst, and C. Pfleiderer, History dependence of the magnetic properties of single-crystal $Fe_{1-x}Co_xSi$, Phys. Rev. B **93**, 235144 (2016).

[18] J. Kindervater, I. Stasinopoulos, A. Bauer, F. X. Haslbeck, F. Rucker, A. Chacon, S. Mühlbauer, C. Franz, M. Garst, D. Grundler, and C. Pfleiderer, Weak crystallization of fluctuating skyrmion textures in MnSi, Phys. Rev. X **9**, 041059 (2019).

[19] N. Manyala, Y. Sidis, J. F. DiTusa, G. Aeppli, D. Young, and Z. Fisk, Magnetoresistance from quantum interference effects in ferromagnets, Nature (London) **404**, 581 (2000).

[20] N. Manyala, Y. Sidis, J. F. DiTusa, G. Aeppli, D. P. Young, and Z. Fisk, Large anomalous Hall effect in a silicon-based magnetic semiconductor, Nat. Mater. **3**, 255 (2004).

[21] S. V. Grigoriev, V. A. Dyadkin, S. V. Maleyev, D. Menzel, J. Schoenes, D. Lamago, E. V. Moskvin, and H. Eckerlebe, Noncentrosymmetric cubic helical ferromagnets $Mn_{1-y}Fe_ySi$ and $Fe_{1-x}Co_xSi$, Phys. Solid State **52**, 907 (2010).

[22] J. Grefe, P. Herre, Y. Hilgers, F. Labbus, N. Lüer-Epping, N. Radomski, M. A. C. de Melo, F. J. Litterst, D. Menzel, and S. Süllow, Near coincidence of metal-insulator transition and quantum critical fluctuations: Electronic ground state and magnetic order in $Fe_{1-x}Co_xSi$, Phys. Rev. B **109**, 054414 (2024).

[23] D. Bloch, J. Voiron, V. Jaccarino, and J. Wernick, The high field-high pressure magnetic properties of MnSi, Phys. Lett. A **51**, 259 (1975).

[24] C. Thessieu, K. Kamishima, T. Goto, and G. Lapertot, Magnetization under high pressure in MnSi, J. Phys. Soc. Jpn. **67**, 3605 (1998).

[25] K. Koyama, T. Goto, T. Kanomata, and R. Note, Observation of an itinerant metamagnetic transition in MnSi under high pressure, Phys. Rev. B **62**, 986 (2000).

[26] R. Ritz, M. Halder, C. Franz, A. Bauer, M. Wagner, R. Bamler, A. Rosch, and C. Pfleiderer, Giant generic topological Hall resistivity of MnSi under pressure, Phys. Rev. B **87**, 134424 (2013).

[27] Y. Nishihara, S. Waki, and S. Ogawa, Mössbauer study of $Mn_{1-y}Fe_ySi$ in external magnetic fields, Phys. Rev. B **30**, 32 (1984).

[28] S. V. Grigoriev, V. A. Dyadkin, E. V. Moskvin, D. Lamago, T. Wolf, H. Eckerlebe, and S. V. Maleyev, Helical spin structure of $Mn_{1-y}Fe_ySi$ under a magnetic field: Small angle neutron diffraction study, Phys. Rev. B **79**, 144417 (2009).

[29] A. Bauer, A. Neubauer, C. Franz, W. Münzer, M. Garst, and C. Pfleiderer, Quantum phase transitions in single-crystal $Mn_{1-x}Fe_xSi$ and $Mn_{1-x}Co_xSi$: Crystal growth, magnetization, ac susceptibility, and specific heat, Phys. Rev. B **82**, 064404 (2010).

[30] S. V. Grigoriev, E. V. Altynbaev, S.-A. Siegfried, K. A. Pschenichnyi, D. Menzel, A. Heinemann, and G. Chaboussant, Spin-wave stiffness in the Dzyaloshinskii-Moriya helimagnets $Mn_{1-y}Fe_ySi$, Phys. Rev. B **97**, 024409 (2018).

[31] A. Petrova, S. Gavrilkin, G. Rybalchenko, D. Menzel, I. Zibrov, and S. Stishov, Physical properties of $(Mn_{1-x}Co_x)Si$ at $x \approx 0.060 - 0.100$: Quantum criticality, Phys. Rev. B **103**, L180401 (2021).

[32] S. Stishov, A. Petrova, D. Menzel, and A. Belemuk, Quantum criticality features in the Co,Fe doped MnSi, Physica B **675**, 415607 (2024).

[33] Y. Fang, S. Ran, W. Xie, S. Wang, Y. S. Meng, and M. B. Maple, Evidence for a conducting surface ground state in high-quality single crystalline FeSi, Proc. Natl. Acad. Sci. **115**, 8558 (2018).

[34] K. E. Avers, Y. S. Eo, H. Yoon, J. A. Horn, S. R. Saha, A. Suarez, P. Zavalij, and J. Paglione, Disordered two-dimensional ferromagnetism at the surface of FeSi, Phys. Rev. B **110**, 134416 (2024).

[35] S. Grigoriev, N. Chubova, L. Azarova, and O. Utesov, Transition from spiral to ferromagnetic structure in $Fe_{1-x}Co_xSi$ compounds: Small-angle neutron scattering study, Ann. Phys. **447**, 169132 (2022).

[36] L. J. Bannenberg, F. Qian, R. M. Dalgliesh, N. Martin, G. Chaboussant, M. Schmidt, D. L. Schlagel, T. A. Lograsso, H. Wilhelm, and C. Pappas, Reorientations, relaxations, metastabilities, and multidomains of skyrmion lattices, Phys. Rev. B **96**, 184416 (2017).

[37] Y. Luo, S.-Z. Lin, D. M. Fobes, Z. Liu, E. D. Bauer, J. B. Betts, A. Migliori, J. D. Thompson, M. Janoschek, and B. Maiorov, Anisotropic magnetocrystalline coupling of the skyrmion lattice in MnSi, Phys. Rev. B **97**, 104423 (2018).

[38] T. Adams, M. Garst, A. Bauer, R. Georgii, and C. Pfleiderer, Response of the skyrmion lattice in MnSi to cubic magnetocrystalline anisotropies, Phys. Rev. Lett. **121**, 187205 (2018).

[39] J. Kindervater, T. Adams, A. Bauer, F. X. Haslbeck, A. Chacon, S. Mühlbauer, F. Jonietz, A. Neubauer, U. Gasser, G. Nagy, N. Martin, W. Häußler, R. Georgii, M. Garst, and C. Pfleiderer, Evolution of magnetocrystalline anisotropies in $Mn_{1-x}Fe_xSi$ and $Mn_{1-x}Co_xSi$ as inferred from small-angle neutron scattering and bulk properties, Phys. Rev. B **101**, 104406 (2020).

[40] M. Preißinger, K. Karube, D. Ehlers, B. Szigeti, H.-A. Krug von Nidda, J. S. White, V. Ukleev, H. M. Ronnow, Y. Tokunaga, A. Kikkawa, Y. Tokura, Y. Taguchi, and I. Kezsmarki, Vital role of magnetocrystalline anisotropy in cubic chiral skyrmion hosts, npj Quantum Mater. **6**, 65 (2021).

[41] N. Akulov, Zur Quantentheorie der Temperaturabhängigkeit der Magnetisierungskurve, Z. Phys. **100**, 197 (1936).

[42] H. Callen and E. Callen, The present status of the temperature dependence of magnetocrystalline anisotropy, and the l(l+1)2 power law, J. Phys. Chem. Solids **27**, 1271 (1966).

[43] A. Chacon, L. Heinen, M. Halder, A. Bauer, W. Simeth, S. Mühlbauer, H. Berger, M. Garst, A. Rosch, and C. Pfleiderer, Observation of two independent skyrmion phases in a chiral magnetic material, Nat. Phys. **14**, 936 (2018).

[44] M. Halder, A. Chacon, A. Bauer, W. Simeth, S. Mühlbauer, H. Berger, L. Heinen, M. Garst, A. Rosch, and C. Pfleiderer, Thermodynamic evidence of a second skyrmion lattice phase and tilted conical phase in Cu_2OSeO_3, Phys. Rev. B **98**, 144429 (2018).

[45] L. J. Bannenberg, H. Wilhelm, R. Cubitt, A. Labh, M. P. Schmidt, E. Lelièvre-Berna, C. Pappas, M. Mostovoy, and A. O. Leonov, Multiple low-temperature skyrmionic states in a bulk chiral magnet, npj Quantum Mater. **4**, 11 (2019).

[46] M. Crisanti, A. O. Leonov, R. Cubitt, A. Labh, H. Wilhelm, M. P. Schmidt, and C. Pappas, Tilted spirals and low-temperature skyrmions in Cu_2OSeO_3, Phys. Rev. Res. **5**, 033033 (2023).

[47] S. Seki, X. Z. Yu, S. Ishiwata, and Y. Tokura, Observation of skyrmions in a multiferroic material, Science **336**, 198 (2012).

[48] S. Seki, J.-H. Kim, D. S. Inosov, R. Georgii, B. Keimer, S. Ishiwata, and Y. Tokura, Formation and rotation of skyrmion crystal in the chiral-lattice insulator Cu_2OSeO_3, Phys. Rev. B **85**, 220406 (2012).

[49] A. Aharoni, Demagnetizing factors for rectangular ferromagnetic prisms, J. Appl. Phys. **83**, 3432 (1998).

[50] J. H. van Vleck, On the anisotropy of cubic ferromagnetic crystals, Phys. Rev. **52**, 1178 (1937).

[51] L. Ludgren, O. Beckman, V. Attia, S. P. Bhattacheriee, and M. Richardson, Helical spin arrangement in cubic FeGe, Phys. Scr. **1**, 69 (1970).

[52] I. Stasinopoulos, S. Weichselbaumer, A. Bauer, J. Waizner, H. Berger, S. Maendl, M. Garst, C. Pfleiderer, and D. Grundler, Low spin wave damping in the insulating chiral magnet Cu_2OSeO_3, Appl. Phys. Lett. **111**, 032408 (2017).

[53] S. M. Sauther, De Haas–van Alphen effect and magnetic anisotropy in correlated electron systems studied by cantilever magnetometry, Ph.D. thesis, Technische Universität München (2021).

[54] R. Skomski, A. Kashyap, A. Solanki, A. Enders, and D. J. Sellmyer, Magnetic anisotropy in itinerant magnets, J. Appl. Phys. **107**, 09A735 (2010).

[55] A. O. Leonov, G. Gödecke, J. Grefe, S. Süllow, and D. Menzel, Low-temperature skyrmions and spiral reorientation processes in chiral magnets with cubic anisotropy: Guidelines for bridging theory and experiment, Phys. Rev. Res. **8**, 013130 (2026).

[56] S. V. Grigoriev, A. S. Sukhanov, and S. V. Maleyev, From spiral to ferromagnetic structure in B20 compounds: Role of cubic anisotropy, Phys. Rev. B **91**, 224429 (2015).

[57] Y. Onose, N. Takeshita, C. Terakura, H. Takagi, and Y. Tokura, Doping dependence of transport properties in $Fe_{1-x}Co_xSi$, Phys. Rev. B **72**, 224431 (2005).